



# Predicting deformation kinetics and fractures propagation in coal-rock masses using acoustic emission testing

Majid Khan<sup>1,2,3</sup> · Xueqiu He<sup>1,2,3</sup> · Dazhao Song<sup>1,2,3</sup> · Zhenlei Li<sup>1,2,3</sup> · Xianghui Tian<sup>4</sup>

Received: 28 July 2024 / Revised: 20 November 2024 / Accepted: 17 February 2025  
© The Author(s) 2025

## Abstract

The formation of coalesced fractures critically alters the mechanical properties of the surrounding virgin material, significantly changing the stress distribution and deformation behavior of the rock mass. However, understanding the generation mechanism and accurate prediction of rock fracture growth remain challenging in many engineering projects. Despite, wide range of conventional approaches including field investigations, laboratory-scale tests, and numerical modeling, the complex geological conditions hinder their accurate determination. This study introduces a new robust and cost-effective holistic geophysical approach to determine fractures propagation and predict failure in coal-rock masses at laboratory scale applicable across scales. The proposed approach combines rock mechanics and Acoustic Emission (AE) testing systems to make useful correlation between AE source parameters and deformation kinetics. This correlation analyzes the spatiotemporal distribution of AE events to elucidate the evolution of fracture patterns in coal-rock specimens from a complex mining project. Results showed dense and complex fracturing networks within coal specimens due to higher density, compaction, and mechanical strength compared to rock samples. This is indicated by peak acoustic events at 80%–100% load versus minimal events at 0–15% load. Simulated fracture patterns closely matched observed acoustic events, identifying key lineaments (macro-cracks) representing the transition from microcracks to macro-fractures. The convergence of these lineaments indicated intensely deformed zones prone to failure, consistent with previous field investigations. Acoustic parameters describing critical damage revealed an inverse relationship between stress and AE event magnitude. At roughly 70%  $\sigma_{\max}$ , a dramatic fall is seen in acoustic parameters indicated the shift from small-scale to large-scale microfractures, ultimately leading to catastrophic failure of the samples. Furthermore, Single Link Cluster (SLC) analysis demonstrated strong correlation among AE events, spatial correlation length ( $\xi$ ) and information entropy ( $H$ ). Both increased significantly at the onset of loading and fluctuated in proximity to ultimate failure. Using the micro-crack density criterion and 3D-crack growth theory, changes in above parameters verified the cracks transformation process. These findings showed that, the proposed approach compared with the conventional approaches, can improve disaster control and management plans, predict critical failures, and save lives in global mining projects when applied to field-scale studies.

**Keywords** Acoustic emission · Fractures · Rock mechanics · Single link cluster (SLC) · Geophysical methods

✉ Majid Khan  
majid@ustb.edu.cn

✉ Dazhao Song  
songdz@ustb.edu.cn

✉ Zhenlei Li  
lizhenlei@ustb.edu.cn

Xueqiu He  
Hexq@ustb.edu.cn

Xianghui Tian  
txh@cugb.edu.cn

<sup>1</sup> School of Resources and Safety Engineering, University of Science and Technology Beijing, Beijing 100083, China

<sup>2</sup> Key Laboratory of Ministry of Education for Efficient Mining and Safety of Metal Mine, University of Science and Technology Beijing, Beijing 100083, China

<sup>3</sup> Research Institute of Macro-Safety Science, University of Science & Technology Beijing, Beijing 100083, China

<sup>4</sup> School of Engineering and Technology, China University of Geosciences (Beijing), Beijing 100083, China

## 1 Introduction

Disturbances in underground geological systems often cause dynamic failures, threatening excavations with fatalities and production losses due to stress-induced fracturing and geological disasters. The natural distribution of fracture structures within rock masses, influenced by complex geological forces, poses significant risks, making it a major concern for global engineering projects (Zhao et al. 2020). These geo-failures have been widely addressed in the past few decades employing theoretical approaches, experiments, and numerical simulations (Wong et al. 2001; Huang et al. 2016).

Owing to the presence of multi-scale natural fractures and diverse induced fractures leading to dynamic failures in rock masses, their comprehensive characterization becomes of utmost importance (Asadizadeh et al. 2019). Furthermore, elucidating the development and propagation mechanisms of fractures in rock masses is essential for both theoretical advancement of rock mechanics and engineering geological applications (Zhang et al. 2015). To address these risks, researchers globally have focused on monitoring the physical and mechanical behaviors of rock masses, studying buckling failure, fracture propagation, and damage processes under loading (Bobet 2000; Hu et al. 2020). In general, to investigate the damage/failure process in coal-rock mass under loading, various monitoring methods are globally practiced, including microseismic technology (Vinoth and Ajay Kumar 2014), acoustic emission (Codeglia et al. 2017; Du et al. 2020; Tang et al. 2022), ultrasonic pulse technology (Zhang et al. 2016), electromagnetic radiation method (Wang et al. 2011; Song et al. 2016; He et al. 2022), computed tomography (Zengin and Erguler 2022), microwave radiation (Huang et al. 2019), and infrared thermal imaging (Zhao et al. 2023b). Among advanced technologies, Acoustic Emission (AE) stands out as a cost-effective and robust method for studying material deformation and failure due to its non-invasiveness, minimal impact on production, and ability to provide dynamic, continuous time–space measurements. With the help of AE technology, the mechanical properties of geomaterials can be determined by analyzing obtained AE parameters encompassing fractal characteristics, seismological parameter ( $b$ -value,  $M_m$ ),  $P(b)$  value, energy indices, and energy released rate (He et al. 2020; Khadivi et al. 2023; Zhao et al. 2023a).

The AE phenomena involves the release of elastic strain energy as internal fractures grow or merge under external loading. These events are closely tied to rock failure and offer a detailed characterization of microdamage evolution in coal-rock bodies (Li et al. 2022). Owing to highly precise characterization in source localization, extensive

studies have been conducted using AE parameters and their relationship to rock failure process under compression in underground engineering projects. The effective utilization of AE three-dimensional location technology allows for the accurate representation of dynamic spatiotemporal characteristics of coal-rock failure/damage under different external loadings, enabling precise tracking of the major cracks and deriving failure patterns (Chang and Lee 2004; Moradian et al. 2012; Pradhan et al. 2015; Wei et al. 2020). For example, the fractal theory was used to comprehend the structural deformation and rock mechanical behavior establishing positive strong correlation between fractal dimension and stress distribution (Zhang et al. 2018a; Yan et al. 2020; Zhou et al. 2022). The effect of loading rate on AE and energy dissipation during cyclic loading of sandstone suggested that the input energy induces the irreversible initiation and propagation of microcracks (Meng et al. 2016). Zhao et al. (2022) determined the fracture patterns, strength, and deformation mechanism using coupled AE and Digital Image Correlation (DIC) on coal samples under different loading rates delineating the failure process into distinct stages: compaction, stable crack propagation, rapid crack propagation, and unstable crack propagation. Jian-po et al. (2015) investigated the mechanical behavior of granite under uniaxial compression using AE monitoring and the moment tensor (MT) method, offering an analysis of the spatiotemporal evolutionary characteristics and fracture mechanisms under load. AE activity can be regarded as a manifestation of field microseismicity, allowing for the application seismology based derived data analysis to examine stress and deformation during rock failure process. With this motive, to reveal the rock failure mechanism,  $b$ -value of AE events was analyzed during deformation showing microcrack growth in coal-rock bodies under loading (Lockner et al. 1991; Weiss 1997; Zhang et al. 2021). The spatial distribution of AE events and the damage-evolution process of coal specimens under cyclic load were examined through the application of the single-link cluster (SLC) method (Zhang et al. 2018a, b). Additionally, variations in SLC structure and spatial correlation length were discussed in relation to different numbers of load cycles. The successful application of AE technology has significantly advanced underground engineering geological investigations. Given the regional variations in engineering geology and the complexity of acoustic responses in diverse environments, conventional approaches such as physical models and numerical simulations may lack precision. Consequently, integrated methodologies become imperative to address these challenges, accounting for variations in coal/rock geo-mechanical properties.

In addition to the aforementioned studies that predominantly focused on physical characteristics of AE in relation

to addressing rock material damage process, there has been a recent surge in interest in the correlation of AE events. Recently, various cluster analysis methods, including SLC, have emerged as a hot topic in this realm. Originally, the SLC method was introduced (Frohlich and Davis 1990; Davis and Frohlich 1991) and systematically applied globally (Zöller et al. 2001) to investigate earthquake sequences, establishing the connection between individual earthquakes and clusters. Zhang et al. (2018a, b) further extended its application in underground mining to investigate the micro-seismic phenomena. Dynamic geological disasters, encompassing phenomena such as rockburst, coal burst, collapse/subsidence, share common features with natural earthquakes. This leads the authors to hypothesize the existence of prevailing geophysical characteristics and acoustic anomalies, potentially serving as discernible precursors. The coexistence and correlation of geophysical characteristics and AE-based individual fractures as potential precursors in deformation and failure processes, have not been systematically investigated in prior researches. Importantly, the introduction of AE-based fractures as a novel method in this research represents a significant advancement in acoustic

technology for engineering geological investigations. In this study, a novel geophysical approach is introduced to identify cracks in coal and rock samples under uniaxial compression. This new crack identification method is integrated with advanced AE data analysis techniques, including clustering approaches and 3D crack growth theory to predict potential failures. A rock mechanics testing system combined with an AE system is employed to analyze deformation kinetics. The findings provide essential insights into the stability of coal and rock masses, dynamic failure phenomena, and safety assurance in underground engineering projects, with applications extending beyond coal mines to various geotechnical fields.

## 2 Experiment design and descriptions

The process of coal-rock failure under loading is a crucial phenomenon involving the initiation and development of micro-fractures/cracks and localized deformations. These micro-scale features progressively aggregate, interconnect, and propagate, eventually culminating in large-scale failure.

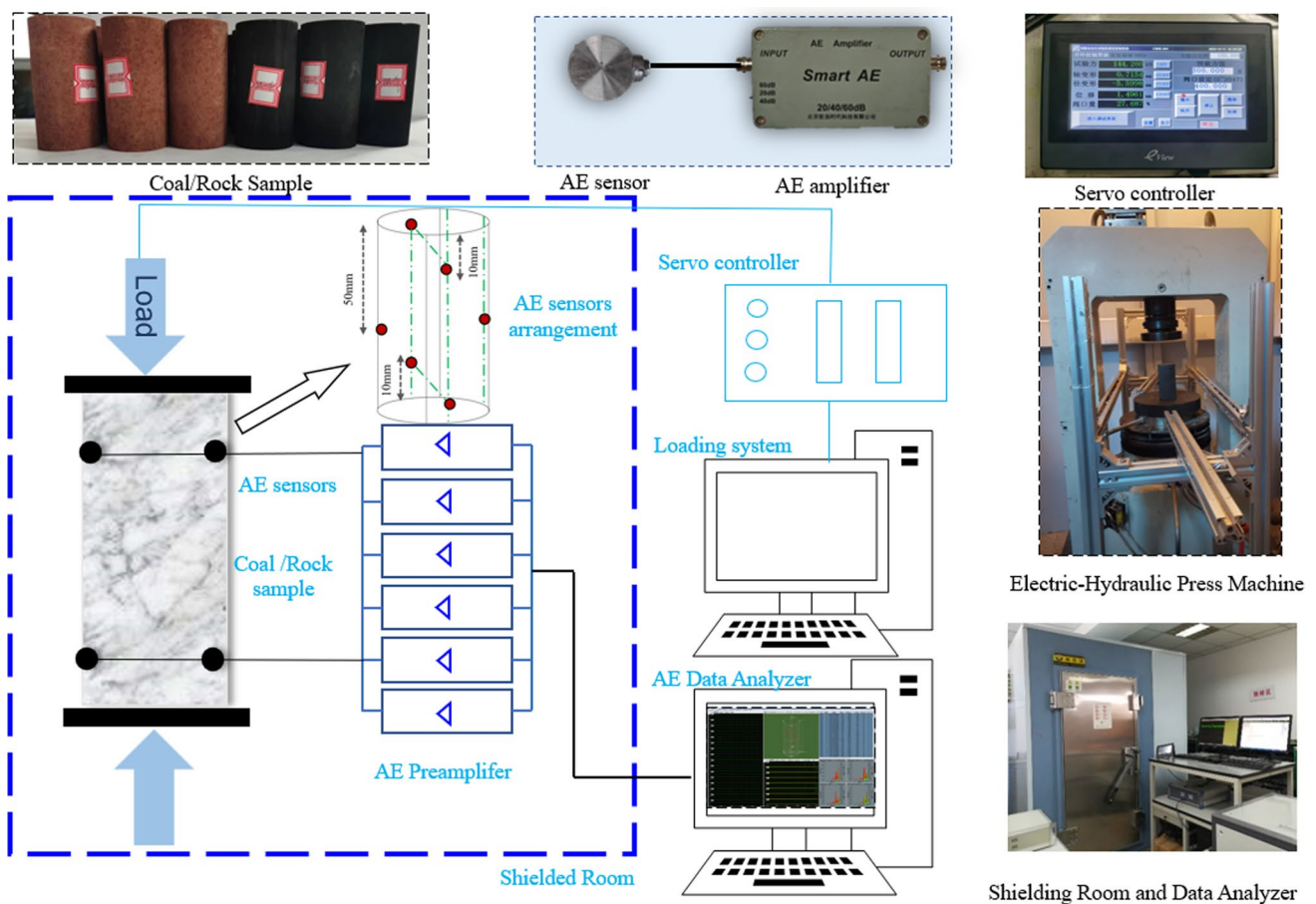


Fig. 1 Schematic representation of experimental system

To comprehend this process, a rock mechanics testing system and an AE test system were employed as shown in Fig. 1. The experimental design system includes AE acquisition system (data analyzer), preamplifier, electrohydraulic press machine, AE sensors, servo controller, loading system, and the shielding room. The AE acquisition system (Micro-II), AE sensors (NANO-30), and preamplifier constitute to the AE location system. The sampling rate was configured at 5MSPS, each AE sensor had a resonant frequency of 300 kHz, and a threshold of 40 dB was applied. The external loads on coal and rock samples were provided by electrohydraulic press machine comprising of 1/300000 of resolution and relative system error of  $\pm 1\%$ . The entire experiment was conducted in the shielding room, providing a shielding effect exceeding 85 dB. This setup aimed to minimize external environmental interference and ensure the accuracy of the experimental results.

The coal and rock samples were collected from a coalmine in Xinjiang Uygur autonomous region to test the proposed methodology of this research. The coal samples consist of anthracite, while the rock samples are red sandstones obtained from the roof of an active coal mine. These samples were prepared in conformity with the guidelines of the International Society for Rock Mechanics (ISRM), involving cutting and polishing into a standard cylindrical form with the recommended dimensions of  $\Phi 50 \times 100$  mm (ISRM, 1978).

Following sample processing, the uniaxial compression test was conducted in a load-control mode, applying a force of 100 N per sample for coal and 300 N per sample for rock specimens. To ascertain the spatiotemporal parameters of AE events, as shown in Fig. 1, a total of six AE sensors were deployed for each experiment, with precise spatial coordinates for positioning. The ultrasonic arbitrary waveform generation card was used to determine the P-wave velocity of both coal and rock samples. The velocity parameters are generally configured within the AE location system based on the measured results. Integrating these parameters with the spatial coordinates of the sensors enables the automatic localization of AE events by the AE location system.

## 3 Methods

### 3.1 Acoustic emission processing

Due to the heterogeneous nature of mineral distribution within rock bodies, the acoustic parameters may vary, making the determination of AE event locations challenging and reliant on the applied algorithm. When considering coal or rock mass as a homogeneous material, a minimum of four sensors is generally required to determine 3D coordinates. However, for increased accuracy, a greater number of AE sensors are necessary. In this study, six sensors were

deployed for precise location determination, utilizing the Geiger localization algorithm to calculate the 3D coordinates of AE signals. The distance of acoustic wave propagation with velocity can be determined using the following equation:

$$\sqrt{(x_i - x_0)^2 + (y_i - y_0)^2 + (z_i - z_0)^2} = v_p (t_i - t_0) \quad (1)$$

Here,  $(x_i, y_i, z_i)$  denotes the coordinates of AE event while  $(x_0, y_0, z_0)$  represents the location coordinates of the source,  $v_p$  is the acoustic wave velocity with arrival and generation times of the AE signal. To enhance accuracy, the AE coordinate vector was adjusted iteratively by modifying the initial vector until the error converged to a minimum value. Following these adjustments, it becomes possible to derive the geometric characteristics of the actual fracture networks.

### 3.2 Stepwise fractures characterization workflow

The complex network of fractures within rock masses serves as a critical determinant in geological failures, influencing the initiation, propagation, and intensity of catastrophic events. Understanding the significance of these fractures is paramount for assessing and mitigating risks in geological and engineering contexts. In general, number of studies have been conducted and methods proposed for fractures mapping in underground engineering geological research (Hencher 2014; Gao et al. 2022; Lu et al. 2022). Previously, Khan et al. (2021) used microseismic data and designed a new workflow for fractures mapping and characterization of field-based microseismicity in a coal mine from China. Expanding upon this methodology, the current research introduces a novel workflow for fractures mapping at a laboratory scale using the AE data representative of microseismic activity.

The systematic workflow for mapping fractures, lineaments, and predicting failure/deformation in coal-rock masses, established in this study, is illustrated in Fig. 2. During the uniaxial compression test, the AE data were processed, and AE event locations were identified, incorporating source location corrections to ensure accuracy and mitigate errors using standard processing procedures. Subsequently, the identified AE events were systematically selected and chronologically sorted, adhering to the typical criteria associated with crack formation, which commonly follows an ascending mode. We innovatively developed the AE-Frac algorithm, which efficiently identifies and categorizes sorted AE events based on their propagation direction, grouping events with the same direction separately from those with different directions. This algorithm employs a polyline to connect events lying in the same direction, thereby facilitating the revelation of fracture patterns. Through this approach, we successfully mapped numerous fractures in different directions by connecting relevant AE events. In this way, numerous fractures with varying

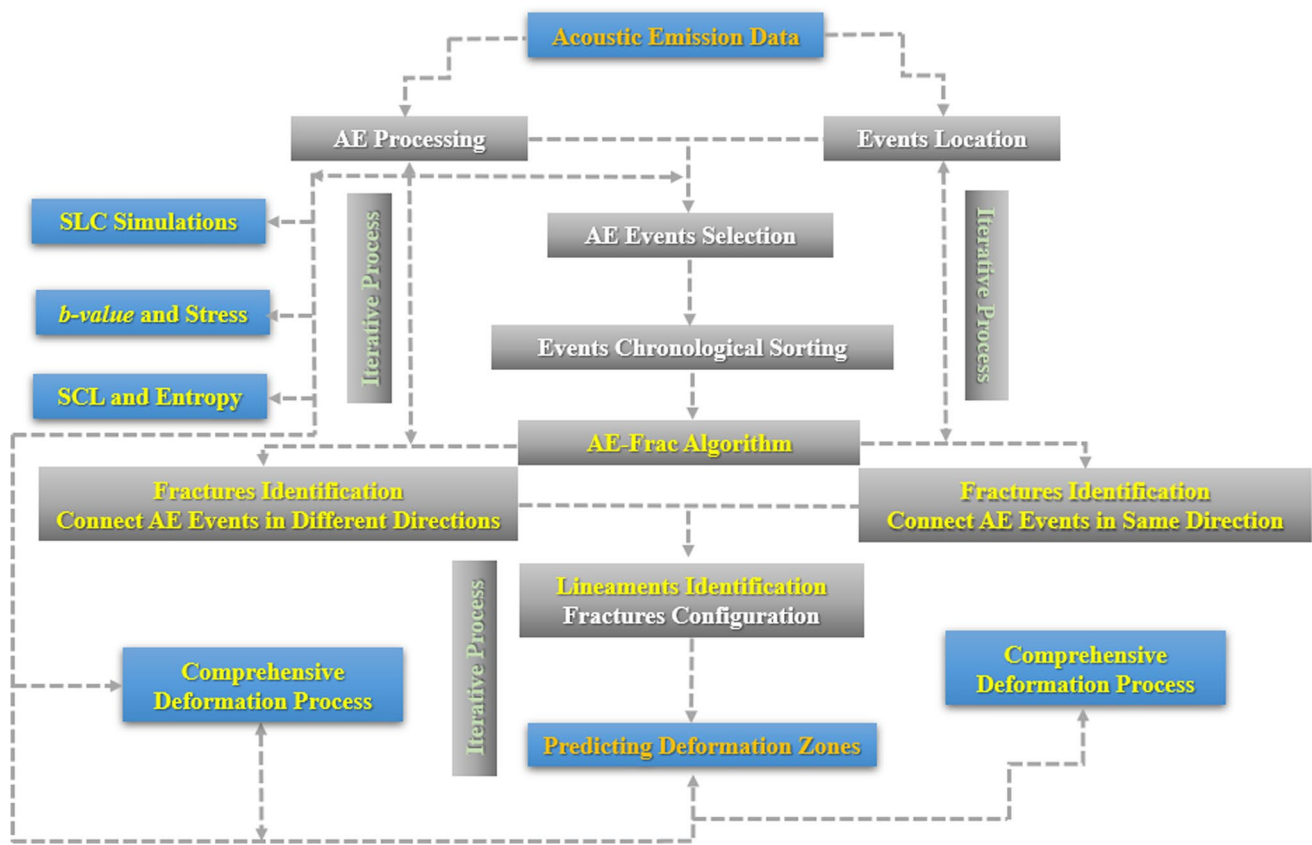


Fig. 2 Workflow of the study conducted

propagation directions are mapped, and utilizing the network and orientation of these fractures, laboratory-scale lineaments are identified by means of established principles of lineament identification in geology. Lineaments serve as linear features in geological representations, indicative of large-scale fractures or similar geological characteristics. Similarly, by tracing the network and configuration of the interpreted lineaments, the regions of deformation and potential failure can be identified. This is achieved through the observation of multiple lineaments converging toward a common point, delineating a weak zone where failure is likely to occur.

This innovative procedure represents a novel, straightforward, cost-effective, and robust method for mapping fractures and to predict failure in geomaterials, including coal and rock, at the laboratory scale. The efficacy of this approach has been validated at the field scale by the authors of this paper in their series of publications (for example see Khan et al. 2021, 2022, 2023a, b).

### 3.3 Governing principles of single link cluster method

The primary working principle of Single Linkage Clustering (SLC) involves calculating the spatiotemporal distances

between AE events. The events exhibiting the shortest temporal-spatial distances to each other are connected, forming individual links between them. Each of these connections represents a single link in the clustering process (Zhang et al. 2018b). In this research, the SLC workflow proposed by Zhou and Liu (2012) in their updated algorithm was employed to construct the SLC structure. The modified workflow is presented in Fig. 2. To begin, a matrix ‘A’ was formed based on the spatiotemporal distances between pairs of AE events, each element  $m_{ij}$  in the matrix, corresponding to the  $i_{th}$  row and  $j_{th}$  column, represents the temporal-spatial distance between the  $i_{th}$  AE event and the  $j_{th}$  AE event. This relationship can be expressed as:

$$m_{ij} = \sqrt{(x_i - x_j)^2 + (y_i - y_j)^2 + (z_i - z_j)^2 + C^2(T_i - T_j)^2} \tag{2}$$

In the above equation, the spatiotemporal distance between pairs of AE events is represented by  $m_{ij}$ , whereas  $x, y$  and  $z$  indicate 3D coordinates of the events,  $C$  shows the temporal-spatial correlation coefficient and  $T$  shows the occurrence time of the AE event. Consider a sequence containing  $N$  AE events. To identify the nearest event for any given event  $s$ , the following process was applied:

- (1) *Comparison within the  $s_{th}$  row*: For each event  $s$  (where  $k = 1, 2, \dots, N$ ;  $k = 1, 2, \dots, N$  and  $k \neq s$ ), every element  $ask$  in the  $s_{th}$  row of matrix  $A$  (representing the temporal-spatial distances) was compared with the other elements in the same row to find the minimum value. Let  $asw$  be the minimum value found, indicating that event  $w$  is the nearest event to event  $s$ .
- (2) *Establishing a single link*: A linear connection (single link) between event  $s$  and event  $w$  was established based on the minimum value  $asw$ .
- (3) *Continued search for nearest event*: Next, the process was repeated for event  $w$  to identify its nearest event using the same method.
- (4) *Generation of SLC subsets*: This iterative searching and linking process resulted in the formation of several SLC subsets, each comprising a cluster of connected AE events based on their proximity in time and space.
- (5) Following the formation of  $M$  subsets (where  $0 \leq M \leq N/2$ ), a new matrix  $B$  was constructed. Each element  $b_{lm}$  in matrix  $B$  represents the spatial distance between subset  $l$  and subset  $m$ , capturing the spatial relationships among these clusters of AE events. This matrix  $B$  serves to analyze and quantify the spatial distribution and clustering patterns within the sequence of events, offering valuable insights into the overall structure of the AE event sequence. This can be mathematically represented as:

$$b_{lm} = a_{uv} = \min(a_{pq}, (u, p\xi l; v, q\xi m)) \quad (3)$$

- (6) Next, we extended the search for the nearest subset of each subset using the algorithm described previously. Utilizing Eq. (3), subset  $m$  was identified as the nearest subset to subset  $l$ , establishing linear connections (single links) between corresponding events  $u$  and  $v$  across subsets  $l$  and  $m$ . Once all these single links between subsets were established, the entire SLC structure was fully assembled, incorporating the spatial relationships and connectivity between subsets to create a comprehensive representation of the clustering and connections within the AE event sequence.

The relationship between cumulative length  $L$  of single links that are shorter than a certain threshold  $l$  and the cumulative length  $L_0$  of all single links follows a Weibull distribution (Zhou and Liu 2012), as expressed by the following equation:

$$w(l) = L/L_0 = 1 - e^{-(l/l_0)^d} \quad (4)$$

According to the Zöller et al. (2001), the spatial correlation length  $\xi$  defined  $w(\xi) = 0.5$ .

## 4 Interpretation of experimental results

### 4.1 Spatiotemporal distribution of AE events/acousticity

The combined rock mechanics and acoustic emission experiment conducted on multiple coal and rock samples resulted in the generation of a large number of AE events. Following data processing and location corrections, the AE events obtained from the coal and rock samples are depicted in Figs. 3a and b, respectively. To facilitate understanding, the distribution of AE events is categorized into different stress states to analyze the geo-mechanical response of coal and rock specimens under varying loads. The data presented for each coal and rock specimen corresponds to different loading stages, ranging from 0%–15%, 15%–30%, 30%–45%, 45%–60%, 60%–80%, and finally 80%–100%. The 80%–100% loading stage represents complete buckling failure of the specimens. This division into loading stages allows for a comprehensive analysis of the material behavior and AE events at different levels of applied stress leading up to failure. The data clearly demonstrate that the coal samples exhibit a higher number of recorded events compared to the rock samples. This difference can be attributed to several factors including density, compaction, presence of primary defects, and distinct mechanical properties inherent to each sample type. The observed variation in AE event counts provides valuable insights into the behavior and response of coal versus rock under applied stress conditions.

During the early loading stage, due to the compression, the closure of primary micropores and microcracks led to minimal AE events, attributed to relative displacement and friction between mineral particles. As stress increased, microcracks developed further, resulting in a progressive increase in AE events which resulted in small-scale local failure. This progressive increase in AE events is attributed to the generation and propagation of microcracks, microscopic structural changes and increased stress contributed to the release of energy. As the stress continues to intensify, the accumulated damage within the material evolves from small-scale microcracks to larger-scale macroscopic fractures. This transition from microfractures to macro-fractures represents a critical stage in the material's failure process, ultimately culminating in structural failure or significant deformation under loading conditions. Subsequently, AE events prominently increased, reaching a peak before the eventual failure of coal and rock samples. This maximum level of AE events signifies the approach towards ultimate failure of the specimens under loading. The occurrence and characteristics of AE events, including their frequency and density, offer valuable insights

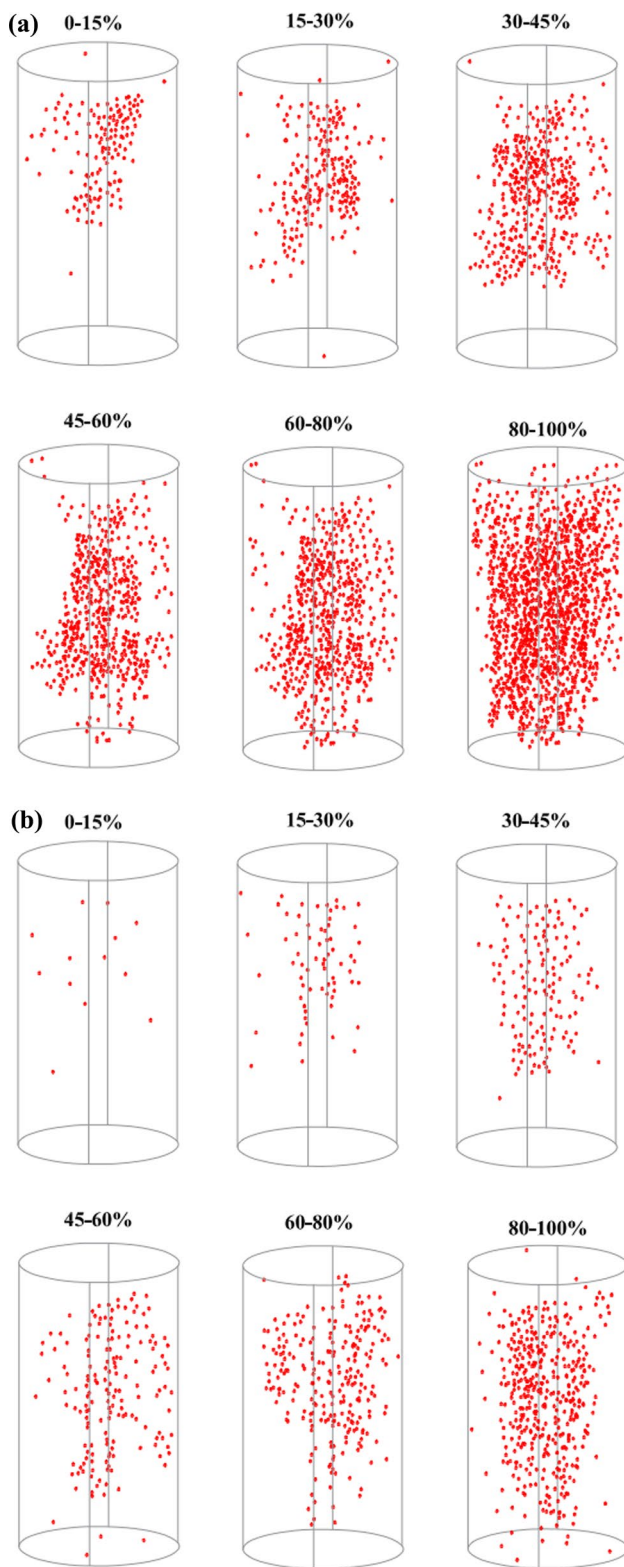


**Fig. 3** **a** Distribution of recorded acoustic emission events in coal sample. **b** Distribution of recorded acoustic emission events in rock sample

into the deformation and failure mechanisms of coal-rock specimens. This phenomenon, resembling microseismicity used for assessing seismic response in coal-rock layers and underground geological structures, helps in comprehensively understanding induced fractures and geological behavior. The authors refer to this approach as “acousticity,” highlighting its significance in studying material behavior under stress conditions.

## 4.2 Fractures characterization

Figure 4a and b illustrate the results of simulated complete fracture networks using the novel methodology introduced in this research, described in Sect. 3.2 and shown in Fig. 2. This representation demonstrates the outcomes of the study, highlighting the effectiveness of the proposed approach in simulating comprehensive fracture networks within the coal and rock specimens examined. We applied this innovative methodology initially to field-scale microseismic data, demonstrating its practicality, and subsequently validated its effectiveness through laboratory-scale acoustic emission testing in the present research. The outcomes of this pioneering workflow include three key aspects: (1) Mapping induced fractures/cracks observed during uniaxial compression testing of coal and rock specimens, (2) Interpreting lineaments representing the transformation from microcracks to macro-fractures, and (3) Predicting potential zones of dynamic failure.

The pattern of mapped fractures for both coal and rock specimens correspond to the AE events monitored during compression test, with the increasing stress/load, both AE events and fractures exhibit corresponding increases. In Fig. 4a, at stress levels of 0%–15% for the coal sample, a smaller number of fractures are observed, primarily located in the upper part of the specimen. This occurrence of fewer fractures is attributed to the closure of primary micropores and microfractures at early stage of the applied stress. Between stress levels of 15%–30% and 30%–45%, there is a significant increase in both the number and frequency of fractures mapped. These fractures exhibit a spread in different directions, corresponding to the occurrence of AE events. Similarly, as stress levels increase up to 80%, additional fractures developed and propagated within the coal specimen. This occurrence intensifies as the specimen undergoes deformation, correlating with the generation and propagation of AE events. In the final stage, approaching complete failure of the specimen, a substantial volume of fractures is observed, consisting of several networks oriented in various directions and encompassing both smaller and larger fractures. It is noteworthy that these simulated fractures offer detailed insights into the internal cracking phenomena that cannot be captured through laboratory

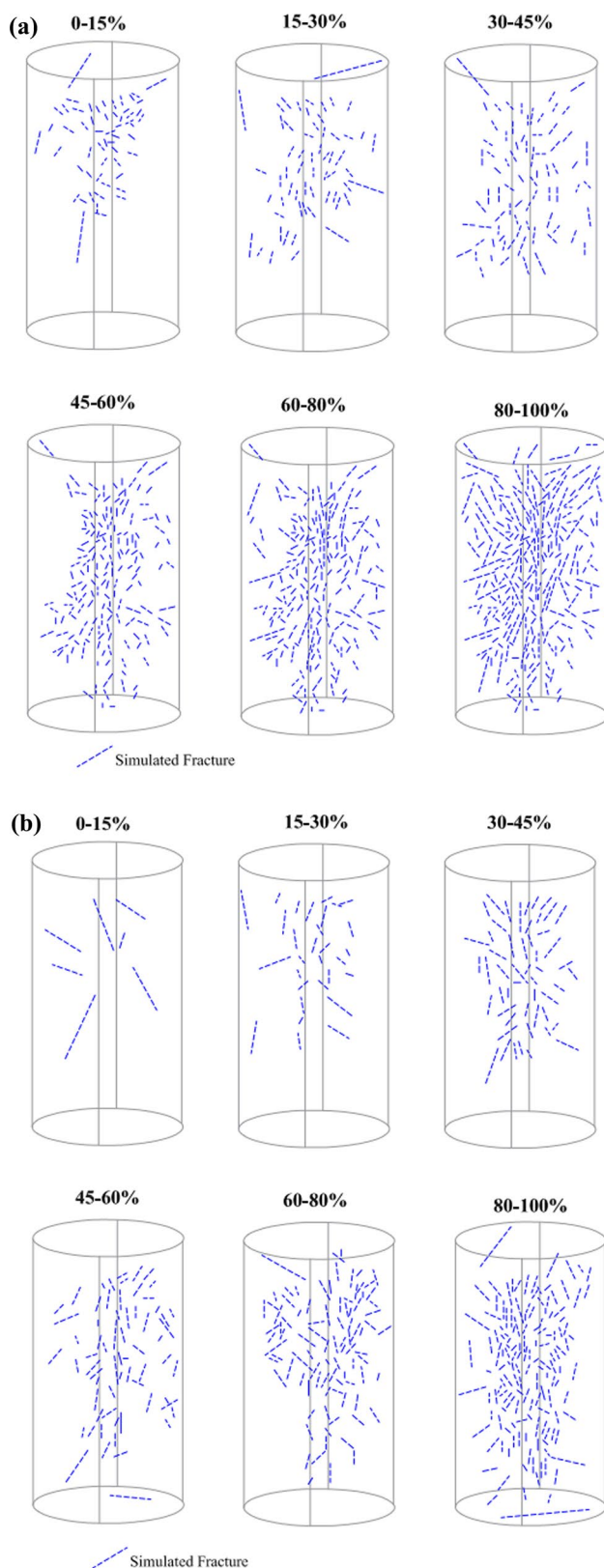


**Fig. 4** a Acoustic emission based simulated fractures in coal sample.  
b Acoustic emission based simulated fractures in rock sample

experiments, thus demonstrating the significance of the proposed methodology.

Similarly, Fig. 4b shows the simulated fractures for a rock sample, which exhibited behavior similar to the coal sample, with the exception of encountering fewer fractures and experiencing a lower degree of failure compared to the coal sample. A total of seven fractures were found at the 0%–15% level, which were longer in length compared to those in the coal sample. This difference is likely due to the distinct geomechanical characteristics of the two specimens. It becomes apparent in subsequent stages leading up to the 80% threshold that the frequency of fracture occurrences gradually intensifies, with a predominant concentration of fractures observed in the upper part of the specimen. The final stage involves the development of an extensive fracture network reaching the bottom of the specimen, resulting in buckling failure. In summary, the simulated fracture process, characterized by various stress levels, includes the closure of preexisting microfractures and micropores, the generation of new fractures, the conversion of microfractures into macrofractures, their propagation, ultimately leading to complete failure.

### 4.3 Complete deformation and disastrous zones prediction

The identification and prediction of dynamic disasters related to engineering geological deformations and failures are complex yet critically important, involving numerous workflows. A crucial step in this process is the comprehensive analysis of AE data to identify the characteristics of AE-based fractures, which serve as precursors to these geological failures. Based on the orientation, configuration, and propagation of simulated fracture networks, various lineaments are identified through proposed simulation workflow as shown in Figs. 5a and b. In geological contexts, lineaments refer to surface expression of subsurface linear geological features such as fractures, fault, and other structural features. In this study, “lineaments” specifically denotes laboratory-scale macrofractures formed through the cumulative propagation of a significant number of fractures in a consistent direction. The identified lineaments correlate with the occurrence of AE events and align with the pattern of induced fractures observed within both coal and rock specimens. Figure 5a illustrates that the coal sample exhibited an increasing number of lineaments with rising stress/time, primarily propagating downward towards the base of the sample with slight variations in propagation directions. During the 60%–80% stress level, the length of lineaments expands, demonstrating propagation in three distinct directions aligned with the deformation propagation direction. As the buckling failure approaches in the final stage, the lineaments along the central part of the sample coalesce and

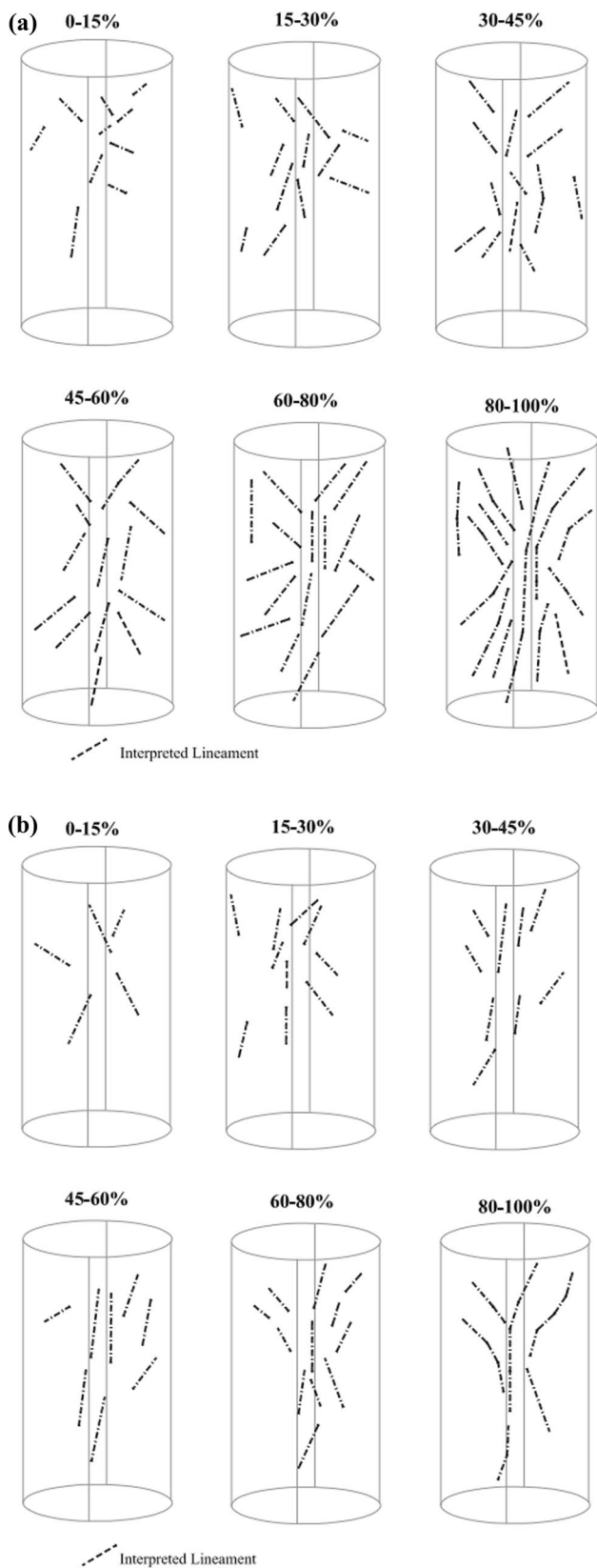


**Fig. 5** **a** Interpreted lineaments in coal sample. *Lineament here represents macro-fractures.* **b** Interpreted lineaments in rock sample. *Lineament here represents macro-fractures*

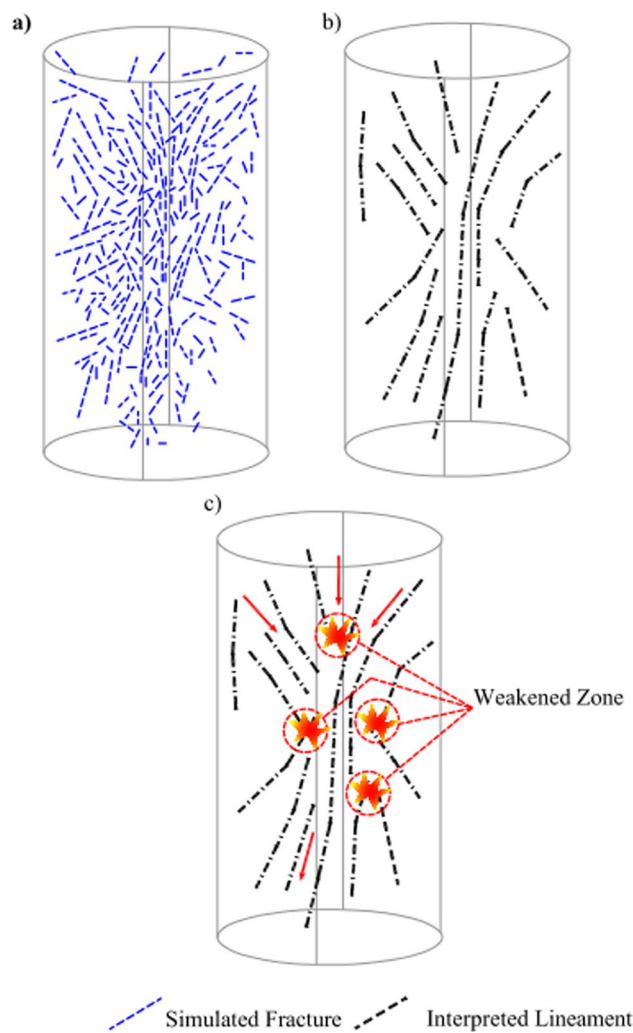


**Fig. 6** Interpreted and predicted deformation model for coal sample. **a** Fracture; **b** Macro-fractures/lineaments; **c** Deformation model

extend downward, indicative of a long-propagated macro-fracture terminating in the complete failure of the coal sample. The coal sample exhibits a total of 14 lineaments oriented in various directions. In contrast to the lineaments observed in the coal sample, those in the rock sample were fewer in number and generally shorter in length. This discrepancy may arise from differences in the acoustic response of the rock's geomechanical characteristics compared to the mapped fractures. As depicted in Fig. 5b, the number of lineaments in the rock sample increases with rising stress levels. Remarkably, at the final stage, smaller lineaments observed in preceding levels merge to form a total of five long lineaments, with one extending to the base of the rock sample. This observation suggests the development of a long-propagated macro-fracture, ultimately leading to the complete failure of the specimen.

Figures 6 and 7 present a comparison of the final stage fractures and lineaments in coal and rock specimens,

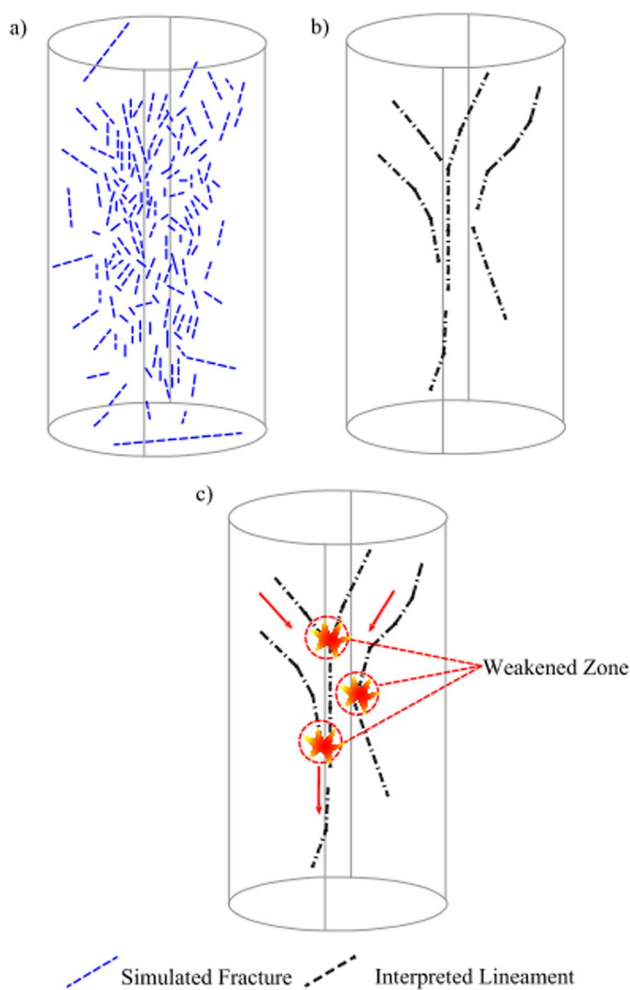


**Fig. 7** Interpreted and predicted deformation model for rock sample

respectively. Interestingly, the observation of simulated fractures and lineaments reveals a pattern wherein lineaments merge towards a central point, indicating several weakened or dangerous zones (for example in Fig. 6c for coal sample). Typically, when multiple fractures or lineaments converge at a single point, it signifies an intensely deformed zone where failure or disaster may occur. This observation aligns with findings from our earlier published works which were based on field investigations using microseismic data, thus confirming the efficacy of our methodology (Khan et al. 2021, 2024). Based on this approach, a total of 4 weakened zones are predicted in coal sample (Fig. 6c) whereas three zones in rock sample (Fig. 7c), also the direction of deformation propagation is indicated with red arrows.

#### 4.4 Evolutionary characteristics of $b$ -value

The laboratory scale evolution of  $b$ -value in AE serves as a vital indicator of structural integrity in engineering feasibility studies. Analogous to its role in earthquake seismology,

$b$ -value variations reflect the tendency for failure, offering insights into material degradation and facilitating proactive maintenance strategies. This connection ( $G$ – $R$  relation) was established by Gutenberg and Richter (1944) describing interrelationship between earthquake magnitudes and their respective frequencies serving as a fundamental framework for assessing the probability of the future seismic events. The  $G$ – $R$  relation can be expressed as:

$$\lg N = a - bM \quad (5)$$

Herein,  $M$  is the magnitude of the earthquake,  $N$  represents the number of events,  $a$ -value shows seismic activity level within a certain time period,  $b$ -value represents the distribution of relative earthquake magnitude. When applied to AE experiment, the  $G$ – $R$  relations enables the calculation of the magnitude of AE event (small earthquake), thereby providing a quantitative measure of the energy release and aiding in the characterization of material behavior under stress which can be computed as:

$$M_{AE} = \log \left( \frac{1}{n} \sum_{i=1}^n (P_i R_i)^2 \right)^{0.5} \quad (6)$$

In the above equation,  $P_i$  and  $R_i$  represent the  $P$ -wave first arrival amplitude and distance of source-receiver for respective sensor  $i$ , respectively. Based on the aforementioned calculations, Fig. 8 illustrates the  $b$ -value and stress variation for both coal and rock specimens. In general, the  $b$ -value is smaller with an increased number of large-amplitude AE events represented by flat line, while a rise in small-amplitude AE events leads to a steeper line and a higher  $b$ -value. As evident from the obtained results in Fig. 8, the  $b$ -value shows nearly similar pattern of variation for both coal and rock specimen with respect to stress change. Initially, high  $b$ -values dominant the distribution, however, to facilitate understanding, the trend of change is divided into three stages: initially, at the onset of applied stress, there is a noticeable non-uniformity in the data; subsequently, a gradual descent stage is characterized by a slow decrease in  $b$ -value as stress increases; and finally, a sharp descent stage indicates an abrupt decrease in  $b$ -value with further stress increments. Particularly, at approximately 70%  $\sigma_{max}$ , a sharp decline in  $b$ -value is observed. Consequently, it can be deduced that at laboratory scale, there exists an inverse relation between stress change and  $b$ -value.

In the context of acoustic response, at the onset of initial loading, with increasing  $b$ -value, AE signals with small amplitudes dominate, reflecting significant microfractures and local-scale deformation. Conversely, a decrease in  $b$ -value indicates the dominance of large amplitude events and large-scale microfractures. Similarly, the data trend suggests that the absence of a prominent change in  $b$ -value

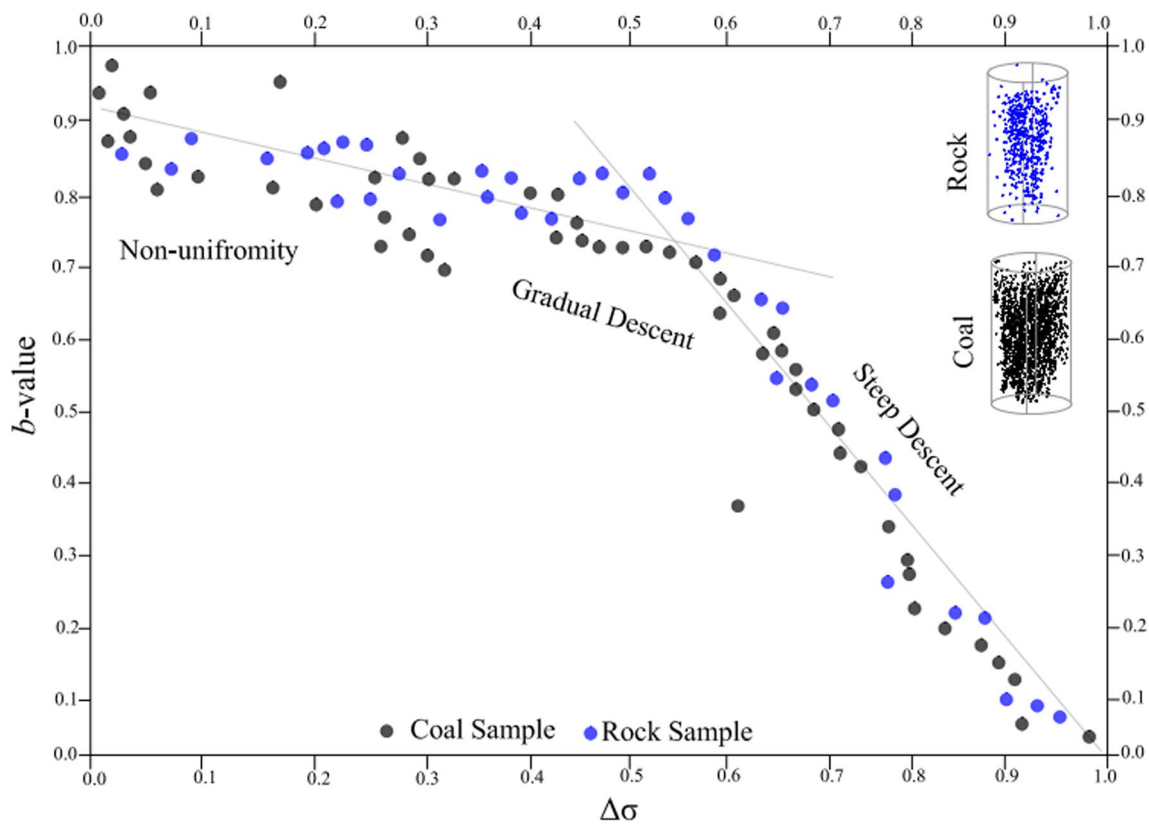


**Fig. 8** Interrelationship between *b*-value and stress under uniaxial loading

indicates a constant occurrence of both small and large-scale microfractures. Similarly, a steep decline or rise in *b*-value over a small range indicates unstable or stable microfracture growth, respectively. In summary, under low stress, in the high and constant *b*-value stages, small-scale microfractures dominate while with the increasing stress change, larger microfractures become more frequent, causing a gradual *b*-value decrease. Finally, a rapid drop in *b*-value at high stress signifies a significant increase in large microfractures, leading to ultimate failure. Consequently, *b*-value of AE serves as a valuable indicator of microfracture evolution within coal and rock specimens. A high and stable *b*-value signifies the prevalence of small-scale microfractures, whereas a decrease in *b*-value suggests a transition towards dominance by larger microfractures, potentially reflecting an impending shift in the deformation process.

### 4.5 Single link cluster analysis

In real-world engineering contexts, the instability and failure of rock masses, primarily characterized by cracks, are influenced by the overlapping of multiple crack events, thereby obscuring clear instability criteria (Chen et al. 2023). Employing single-crack identification methodologies offers a viable approach to elucidate these instability

criteria effectively. According to the SLC method described in Sect. 3.3, the SLC structures of the encountered AE events (Figs. 3a and b) were constructed for coal and rock specimens as shown in Figs. 9 and 10, respectively. In these figures, the red lines indicate the shortest distance between the AE events whereas the red color represents the single links between SLC subsets. Interestingly, the patterns obtained from SLC simulation and novel fracture methodologies closely resemble each other, demonstrating the effectiveness of integrating these two workflows for fracture generation, propagation, and deformation analysis. Compared to the rock sample, the coal sample exhibits denser clustering corresponding to AE events, particularly during the ultimate failure stage (80%–100%). The single links and their subsets are predominantly concentrated and merged together, indicating complex internal fracturing and deformation processes within the coal sample. In the rock sample, the links are longer in length, predominantly composed of single links. In general, it is evident that the number of AE events and the SLC structures in both samples exhibit positive correlation.

The SLC structure spontaneously represents the deformation propagation process in coal and rock specimens. However, to obtain more profound and meaningful insights, the statistical characteristics of the SLC structure are crucially

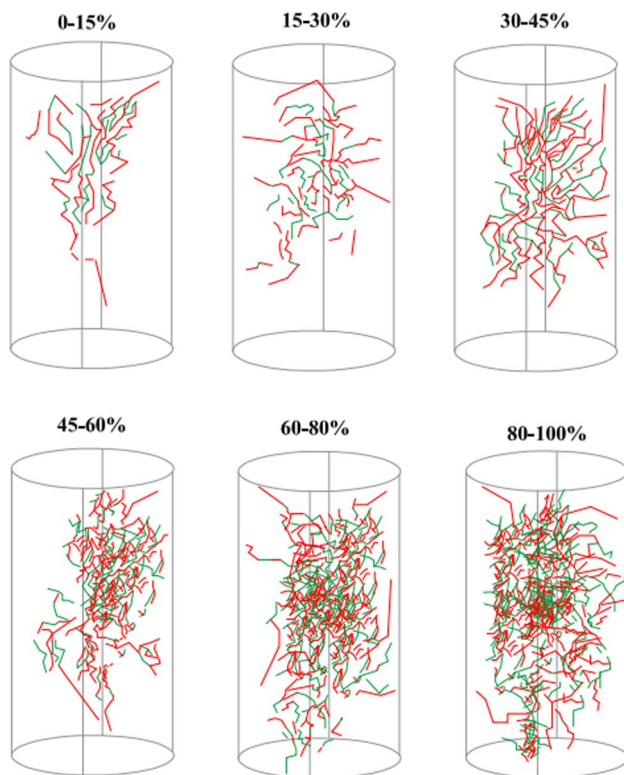


Fig. 9 SLC structure of coal sample

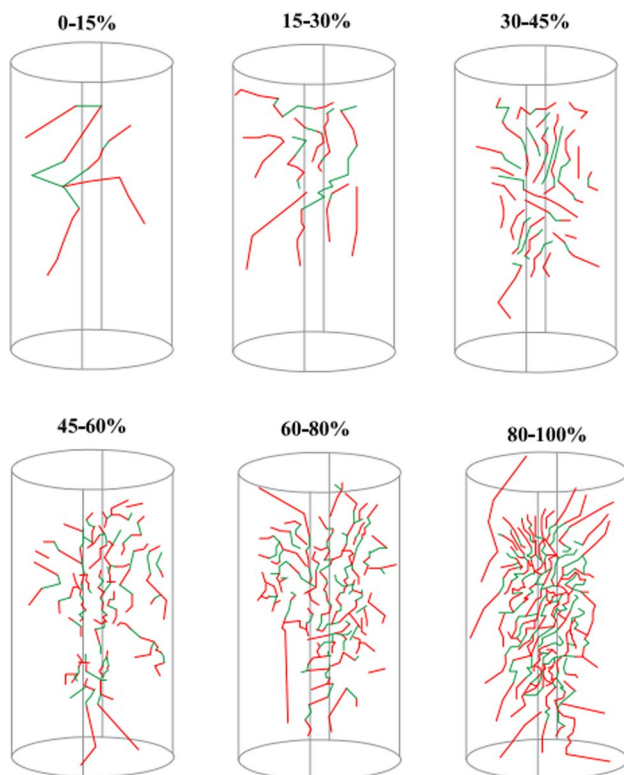


Fig. 10 SLC structure of rock sample

important. Furthermore, through the construction of SLC structure, the spatial correlation lengths  $\xi$  and information entropy  $H$  of the AE events for both coal and rock samples were computed. The spatial correlation length  $\xi$  is defined in Eq. (4). The information entropy  $H$  describes the average information contained in each piece of received information serving as a measure of uncertainty. In the domain of information, higher entropy corresponds to a greater amount of information being transmitted. The information entropy was computed using the following equation:

$$H(X) = E[1(X)] = [-\ln(P(X))] \quad (7)$$

Herein,  $H$  represents the information entropy in amount of  $X$ ,  $P$  shows the probability of mass function of  $X$ , while  $E$  represents the expectation function and  $I(X)$  is the information amount. For finite number of samples, the entropy can be written as:

$$H(X) = \sum_i^n P(x_i)I(x_i) = -\sum_i^n P(x_i) \log_{\beta} P(x_i) \quad (8)$$

The parameter in the logarithmic function represents the logarithmic base, determining the unit of entropy. The unit of entropy varies with the value of this base, which is influenced by the parameter  $\beta$ . According to the principles of information entropy, a discrete distribution of link lengths within the SLC structure results in high entropy. In contrast, a concentrated distribution of link lengths leads to low entropy. Utilizing the above methodology, the spatial correlation length  $\xi$  and information entropy  $H$  for the AE events were computed and analyzed during the process of applied load as presented in Figs. 11 and 12 (coal and rock samples, respectively). The data trend exhibits three distinct stages: a fluctuating stage with low intensity, a gradual increase with moderate intensity, and an abrupt increase with high intensity. These stages correspond to the increasing changes in stress. For the coal sample as shown in Fig. 11, the spatial correlation length ( $\xi$ ) increased gradually at the beginning of uniaxial loading. This parameter then showed fluctuations between 40%  $\sigma_{max}$  and 75%  $\sigma_{max}$ . An upward trend in  $\xi$  reappeared just before the coal sample experienced buckling failure. At the same time, the information entropy  $H$  fluctuated throughout most of the loading process, however, it began to decrease when the stress reached approximately 65%  $\sigma_{max}$ . While, for the rock sample as shown in Fig. 12, the spatial correlation length ( $\xi$ ) showed gradual fluctuations between 50 to 80% of  $\sigma_{max}$  and then an abrupt increase with high intensity until the ultimate failure. The information entropy didn't show a pronounced change; however, an abrupt decline is seen after 90%  $\sigma_{max}$ . In general, the rock sample exhibited similar trends for both parameters, with the key difference being that the

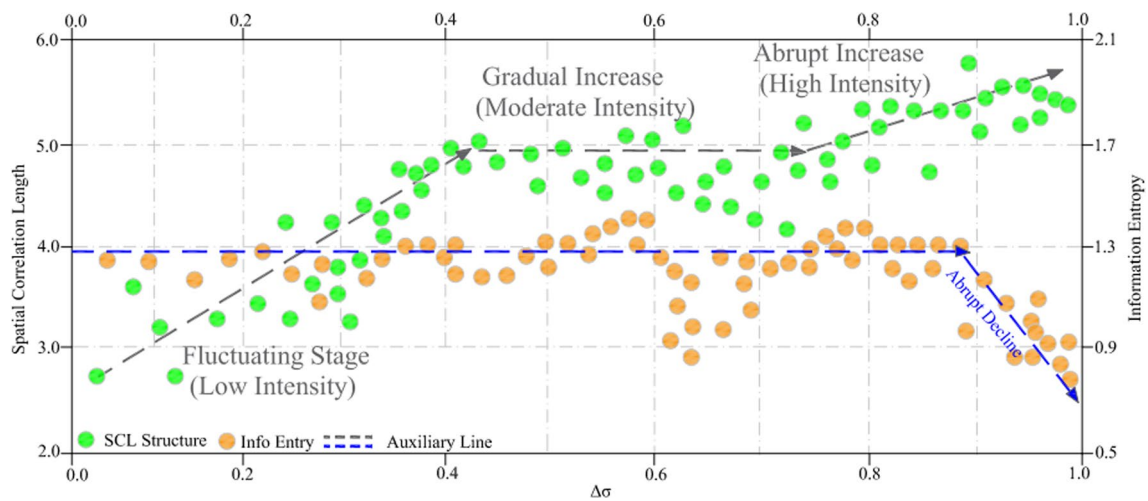


Fig. 11 The spatial correlation length and information entropy for coal sample

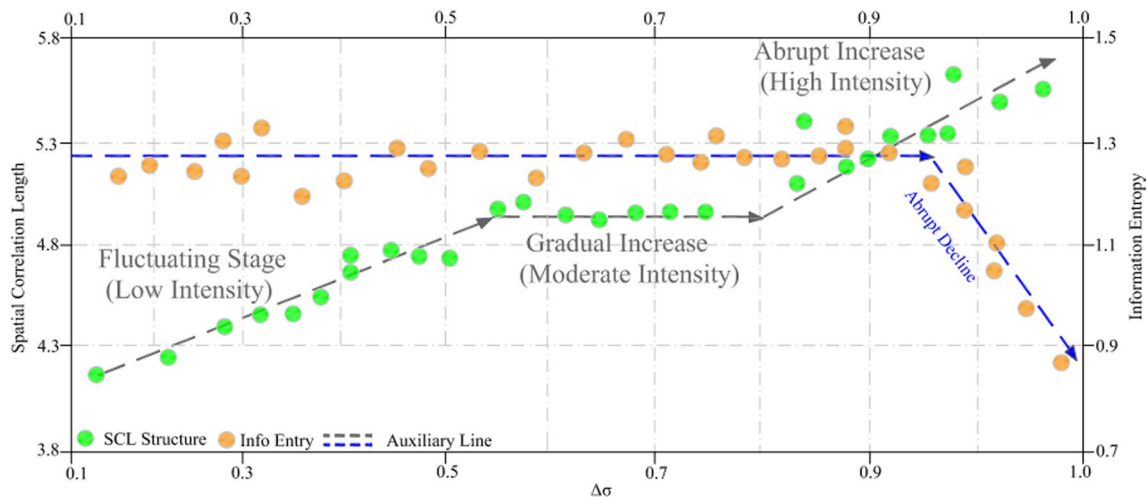


Fig. 12 The spatial correlation length and information entropy for rock sample

initial upward phase for  $\xi$  started and ended later than in the coal sample. Analyzing the trends of these parameters, it is observed that the  $b$ -value (Fig. 8) remains relatively stable during the initial loading phase, whereas the spatial correlation length ( $\xi$ ) demonstrates a marked increase at the beginning. Unlike  $b$ -value and  $\xi$ , the information entropy ( $H$ ) does not show significant sensitivity to the failure of the coal and rock samples throughout most of the loading process. Nonetheless, it is noteworthy that all three parameters— $b$ -value, spatial correlation length ( $\xi$ ), and information entropy ( $H$ )—undergo substantial changes just before the buckling failure of the samples.

### 5 Critical discussion

In laboratory settings, AE technology has been proven to be crucial for investigating fracture propagation, micro-rack to macro-fracture transformation process, and deformation in coal and rock samples. This analysis provides essential insights into the geomechanical behavior of coal and rock masses at the field scale, aiding in the accurate modeling of predicting engineering failures and dynamic disasters. Despite global advancements in measurement technologies and modeling, overlooking diverse prediction

methods risks societal safety, emphasizing the necessity of thoroughly characterizing fracture behavior and prediction efficacy for improved dynamic disaster control (Shah and Labuz 1995; Brnich and Kowalski-Trakofker 2010; Molinda and Mark 2010; Tan et al. 2023). This research presents a comprehensive approach that integrates theoretical fracture mechanics with a newly developed geophysical method for lab-scale fracture mapping, offering enhanced insights into the dynamic failure of coal and rock samples under uniaxial compression.

The mapped fracture patterns for coal and rock specimens correlated with AE events monitored during compression tests. Initially, coal samples show few fractures due to micropore closure, however, the fracture frequency increases significantly at higher stress levels, forming extensive networks before complete failure. Rock samples exhibit fewer, longer fractures initially, with intensified frequency leading to buckling failure. The heterogeneity of coal and rock samples, particularly their distinct densities and fracture complexities, significantly influenced the observed fracture networks and AE event distributions. Coal's lower strength, higher brittleness, and inherent anisotropy contributed to its denser and more complex fracture networks, as compared to rock samples. These material properties also led to a higher frequency and more diverse orientation of AE events in coal specimens under increasing stress levels. In contrast, the stronger and less brittle rock samples exhibited fewer fractures and lower AE event densities. Preexisting microfractures in coal further amplified its mechanical response to loading, accelerating the transition from microfractures to macrofractures. These findings not only elucidate the material-specific behavior observed in laboratory conditions but also highlight critical factors influencing failure mechanisms under field conditions, aiding in the prediction of dynamic failure zones. While the experiments were conducted in a controlled environment, differences from real underground conditions remain. Factors such as temperature and humidity, which affect the mechanical properties of coal and rock, were not fully replicated. For example, elevated temperatures may weaken material strength, while high humidity can reduce coal's strength and increase deformability due to its porous nature. Additionally, laboratory loading conditions cannot fully mimic the multi-axial stresses and dynamic loads present in the field. Future studies incorporating these variables are essential to bridge the gap between laboratory findings and field applications.

Identified lineaments in both samples align with AE events, indicating intensely deformed zones prone to failure, validated by earlier field investigations using microseismic data. When these lineaments (macrofractures) converge at a single point, it signifies a potentially dangerous zone characterized by increased fracturing intensity and frequency. This novel method of mapping fractures in coal-rock specimens

highlights the importance of AE data analysis in predicting geological failures at the lab scale, which is equally significant at the field scale.

The fracture propagation in a material is a complex process influenced by longitudinal shear, with some researchers suggesting that secondary microfractures in the specimen may cease to propagate beyond halfway along the length of the primary fracture (Dyskin et al. 2021). The buckling failure of rock material is attributed to the interaction of microcracks, a phenomenon essential for microcrack growth theory (Zhurkov et al. 1984), which posits that the propagation and coalescence of these microcracks play a pivotal role in the structural integrity of the material. With this motive the Microcrack Density calculation criterion is used to analyze the microcrack growth and transformation process, which can be computed as:

$$M = S/D \quad (9)$$

where  $S$  represents the average spacing of the microfracture/crack,  $D$  is the microfracture scale and  $M$  defines the interrelationship between these two parameters. With a random distribution of microfractures in a given area, if the microcrack is represented by ( $f$ ), then the probability ( $P_m$ ) can be computed as:

$$P_f \propto \left(\frac{e}{M}\right)^f \quad (10)$$

Analyzing the data obtained from uniaxial compression tests, the relative growth of microfractures is not pronounced at the onset of loading. However, within specific areas, the microfracture density shows a significant increase, indicating the transformation process of microfractures. This transformation leads to the development of macrofractures, ultimately facilitating the failure of the entire coal and rock samples.

The  $b$ -value of AE events serves as an indicator of the distribution of both large-amplitude and small-amplitude acoustic events, providing insight into variations in microfracture scale. Under low stress conditions (onset of uniaxial compression), AE events primarily arose from the closure and growth of microfractures. Given the relatively small scale of microfractures, small-amplitude AE events predominated, contributing to a high  $b$ -value. As stress levels rise, interactions between smaller-scale microfractures facilitated the formation of larger-scale microfractures. Consequently, the occurrence of large-amplitude acoustic events increased within a narrow range, resulting in a gradual decrease in the  $b$ -value as the microfracture state evolves slowly. During the later stages of loading, the cumulative effect of microfractures interactions lead to the proliferation of larger-scale microfractures, culminating in the ultimate failure of coal and rock specimens. This phase witnesses a prominent

increase in large-scale microfractures, manifesting as a rapid increase in large-amplitude AE events and a corresponding conspicuous decrease in the  $b$ -value. In summary, variations in the  $b$ -value of AE events provide valuable insights into the evolving microfracture dynamics and impending failure mechanisms of coal and rock samples under varying stress conditions.

According to analysis of the SLC, the microfracture clusters determine the stable crack locations. Data analysis revealed that areas with low intensity exhibit a substantial accumulation of energy, facilitating the proliferation of microfractures, evidenced by a pronounced increase in number of microfractures and the occurrence of acoustic events. In contrast, regions with high intensity restricted the microfractures formation, resulting in a discernible reduction in microfracture growth and acoustic events compared to areas with lower intensity. According to the fundamental principles of SLC theory, it is observed that AE events resulting in former stage tend to create single links characterized by short link lengths whereas AE events stemming from the later stage tend to form single links with longer link lengths. Summarizing the SLC discussion, it is inferred that the crack evolution during instability involves three stages: small-scale microfractures (divergence in linear deformation), large-scale microfractures (convergence during microcrack growth) and transformation into macro-fractures (disorder after macrocrack formation).

The intrinsic heterogeneity within coal-rock specimens is often discernible through the prevalence of primary microfractures, evidenced by the accumulation of acoustic events. In this context, the analysis of computed spatial correlation length  $\xi$  emerges as a robust and insightful parameter, facilitating a deeper understanding of fracture propagation mechanisms. Initially, as stress increased,  $\xi$  gradually increased, reflecting the expansion of locally deformed regions. Subsequently,  $\xi$  stabilized as microfractures grew and interacted within these areas. At the end of applied load, intensified microfractures interactions led to the extension of the deformed area, resulting in a renewed increase in  $\xi$ . The information entropy ( $H$ ) generally represents the respective changes in the direction of propagation of microfractures where high  $H$  and low aggregation degree show various combination modes depending upon the location uncertainty of microfractures. Thus, an abrupt increase/decrease in information entropy is indicative of catastrophic event or ultimate failure. The information entropy in general remained higher with the increasing load, however, an abrupt decrease occurred at 90% of the stress change before the ultimate failure of the samples. This sudden decrease represents interconnectedness of the microfracture and formation of large fracture. This analysis of entropy helps in knowing the fractures evolutionary mechanism. In summary, as evident by the observed changes in various AE

parameters, the entire deformation and failure of the coal and rock specimens represents small-scale to large-scale fracture transformation and local-scale deformation to ultimate failure. This holistic approach consisting of newly introduced fractures mapping methodology and existing clustering analysis, while a panacea for monitoring deformation process holds a significant meaning in understanding the acoustic response of subsurface coal-rock layers ultimately assisting researchers and industry practitioners in predicting geological failures in underground engineering projects.

Building upon existing metrics such as SCL  $\xi$  and  $H$ , this study presents a novel methodology that integrates advanced AE analysis with a systematic framework for crack identification, propagation, and failure prediction. By combining these elements, the study provides a new lens to examine the dynamic evolution of fractures, capturing the transition from microcrack interactions to macro-scale fracture networks under uniaxial stress conditions. This methodology identifies critical stress thresholds where AE event clustering intensifies, marking the onset of significant structural transformations. The ability to track and correlate these changes with deformation kinetics offers a robust framework for predicting failure mechanisms with greater accuracy. By extending traditional fracture characterization techniques, this approach delivers an efficient and scalable method applicable to both experimental and field-scale studies.

## 6 Conclusions and recommendation

This study integrates AE analysis with a novel crack identification methodology and theoretical fracture mechanics, providing a holistic framework for examining the transformation from micro-cracks to macro-cracks and their role in failure mechanisms. By linking these transformations to fracture evolution, the research offers valuable insights into the dynamic deformation processes of coal and rock samples under uniaxial compression and practical applications for predictive modeling and disaster management in underground engineering.

The mapped fracture patterns of coal and rock specimens, using a novel methodology, showed distinct behaviors under different stress levels. Coal samples initially had few fractures due to micropore closure. At higher stress levels, fracture frequency increased significantly, forming extensive networks before buckling failure. Rock samples, in contrast, exhibited fewer but longer fractures at first, with frequency rising before buckling failure. Identified lineaments, aligned with AE events, indicated intensely deformed zones prone to failure. This observation was validated by previous field investigations using microseismic data. These results confirm the effectiveness of AE data analysis in predicting geological failures at both

laboratory and field scales. The transformation of microfractures into macro-fractures is crucial for understanding the structural integrity and failure of coal and rock materials. The Microcrack Density calculation criterion provided key insights into the growth and coalescence of microfractures, highlighting the underlying mechanisms of failure. Initially, microfracture density remains low but increases significantly in localized areas under stress, leading to the formation of macro-fractures and eventual sample failure. The analysis of the  $b$ -value of AE events also provided valuable information on microfracture dynamics and impending failure under varying stress conditions. Spatial correlation length ( $\xi$ ) analysis revealed the progressive stages of fracture propagation. Areas with low intensity showed substantial energy accumulation, facilitating the growth of microfractures. In contrast, high-intensity areas restrict their formation. The combined analysis of  $\xi$  and information entropy ( $H$ ) offers further insights into fracture propagation mechanisms, highlighting the intrinsic heterogeneity of coal-rock specimens. High entropy and low aggregation degrees correspond to varied microfracture propagation directions. An abrupt decrease in entropy at 90% of the stress change before failure indicates the formation of large fractures and ultimate sample failure.

The combination of AE data analysis, the newly introduced fracture mapping methodology, and existing clustering analysis provides a comprehensive framework for monitoring deformation in coal and rock samples. This holistic approach offers valuable insights into the acoustic response of subsurface coal-rock layers. It aids researchers and industry practitioners in predicting geological failures in underground engineering projects. These findings advance our understanding of complex fracture behaviors and failure mechanisms, supporting improved modeling, prediction, and control of dynamic disasters in underground engineering.

**Acknowledgements** This research was supported by Beijing Natural Science Foundation (International Scientists Project; Grant No. IS23116) and Research Fund for International Young Scientists (RFIS-I) of National Science Foundation of China (42250410327). The University of Science and Technology Beijing (USTB), Beijing, China is thanked for providing research facilities.

**Author contributions** Majid Khan: Conceived and designed the analysis, performed the analysis, wrote the paper, made edits, and refinements; Xueqiu He: Supervision, Review and Edits; Dazhao Song: Supervision, Review and Edits; Zhenlei Li: Data provision, Review and Edits; Xianghui Tian: Formal analysis, Review and Edits.

**Funding** Beijing Natural Science Foundation (International Scientists Project; Grant No. IS23116).

**Data availability** The data will be available on request.

## Declarations

**Conflict of interest** The authors declare “no competing interest”.

**Open Access** This article is licensed under a Creative Commons Attribution 4.0 International License, which permits use, sharing, adaptation, distribution and reproduction in any medium or format, as long as you give appropriate credit to the original author(s) and the source, provide a link to the Creative Commons licence, and indicate if changes were made. The images or other third party material in this article are included in the article's Creative Commons licence, unless indicated otherwise in a credit line to the material. If material is not included in the article's Creative Commons licence and your intended use is not permitted by statutory regulation or exceeds the permitted use, you will need to obtain permission directly from the copyright holder. To view a copy of this licence, visit <http://creativecommons.org/licenses/by/4.0/>.

## References

- Asadzadeh M, Hossaini MF, Moosavi M et al (2019) Mechanical characterisation of jointed rock-like material with non-persistent rough joints subjected to uniaxial compression. *Eng Geol* 260:105224. <https://doi.org/10.1016/j.enggeo.2019.105224>
- Bobet A (2000) The initiation of secondary cracks in compression. *Eng Fract Mech* 66:187. [https://doi.org/10.1016/S0013-7944\(00\)00009-6](https://doi.org/10.1016/S0013-7944(00)00009-6)
- Brnich MJ, Kowalski-Trakofker KM (2010) Underground coal mine disasters 1900–2010: events, responses, and a look to the future. In: *Extracting the science: a century of mining research*
- Chang SH, Lee CI (2004) Estimation of cracking and damage mechanisms in rock under triaxial compression by moment tensor analysis of acoustic emission. *Int J Rock Mech Min Sci* 41:1069. <https://doi.org/10.1016/j.ijrmmms.2004.04.006>
- Chen Z, Wang P, Shi F (2023) Investigation of crack recognition and spatio-temporal evolution pattern in coal samples damage. *Sci Rep* 13:17961. <https://doi.org/10.1038/s41598-023-45276-z>
- Codeglia D, Dixon N, Fowmes GJ, Marcato G (2017) Analysis of acoustic emission patterns for monitoring of rock slope deformation mechanisms. *Eng Geol* 219:21. <https://doi.org/10.1016/j.enggeo.2016.11.021>
- Davis SD, Frohlich C (1991) Single-link cluster analysis, synthetic earthquake catalogues, and aftershock identification. *Geophys J Int* 104:289. <https://doi.org/10.1111/j.1365-246X.1991.tb02512.x>
- Du K, Li X, Tao M, Wang S (2020) Experimental study on acoustic emission (AE) characteristics and crack classification during rock fracture in several basic lab tests. *Int J Rock Mech Min Sci* 133:104411. <https://doi.org/10.1016/j.ijrmmms.2020.104411>
- Dyskin AV, Pasternak E, Qi C et al (2021) A possible mechanism of failure in dynamic uniaxial compression and the size effect. *Eng Fract Mech* 257:108005. <https://doi.org/10.1016/j.engfracmech.2021.108005>
- Frohlich C, Davis SD (1990) Single-link cluster analysis as a method to evaluate spatial and temporal properties of earthquake catalogues. *Geophys J Int* 100:19. <https://doi.org/10.1111/j.1365-246X.1990.tb04564.x>
- Gao X, Zhang Y, Hu J et al (2022) Site-scale bedrock fracture modeling of a spent fuel reprocessing site based on borehole group in Northwest, China. *Eng Geol* 304:106682. <https://doi.org/10.1016/j.enggeo.2022.106682>
- Gutenberg B, Richter CF (1944) Frequency of earthquakes in California\*. *Bull Seismol Soc Am* 34:185. <https://doi.org/10.1785/bssa0340040185>
- He S, Song D, He X et al (2020) Coupled mechanism of compression and prying-induced rock burst in steeply inclined coal seams and principles for its prevention. *Tunn Undergr Space Technol* 98:103327. <https://doi.org/10.1016/j.tust.2020.103327>

- He S, Qin M, Qiu L et al (2022) Early warning of coal dynamic disaster by precursor of AE and EMR “quiet period.” *Int J Coal Sci Technol* 9:46. <https://doi.org/10.1007/s40789-022-00514-z>
- Hencher SR (2014) Characterizing discontinuities in naturally fractured outcrop analogues and rock core: the need to consider fracture development over geological time. *Geol Soc Spec Publ* 374:113. <https://doi.org/10.1144/SP374.15>
- Hu J, Wen G, Lin Q et al (2020) Mechanical properties and crack evolution of double-layer composite rock-like specimens with two parallel fissures under uniaxial compression. *Theor Appl Fract Mech* 108:102610. <https://doi.org/10.1016/j.tafmec.2020.102610>
- Huang D, Gu D, Yang C et al (2016) Investigation on mechanical behaviors of sandstone with two preexisting flaws under triaxial compression. *Rock Mech Rock Eng* 49:375. <https://doi.org/10.1007/s00603-015-0757-3>
- Huang J, Hu G, Xu G et al (2019) The development of microstructure of coal by microwave irradiation stimulation. *J Nat Gas Sci Eng* 66:86. <https://doi.org/10.1016/j.jngse.2019.03.016>
- International society for rock mechanics commission on standardization of laboratory and field tests (1978) Suggested methods for the quantitative description of discontinuities in rock masses. *Int J Rock Mech Min Sci*. 15
- Jian-po L, Yuan-hui L, Shi-da X et al (2015) Cracking mechanisms in granite rocks subjected to uniaxial compression by moment tensor analysis of acoustic emission. *Theor Appl Fract Mech* 75:151. <https://doi.org/10.1016/j.tafmec.2014.12.006>
- Khadivi B, Heidarpour A, Zhang Q, Masoumi H (2023) Characterizing the cracking process of various rock types under Brazilian loading based on coupled acoustic emission and high-speed imaging techniques. *Int J Rock Mech Min Sci* 168:105417. <https://doi.org/10.1016/j.ijrmms.2023.105417>
- Khan M, He X, Farid A et al (2021) A novel geophysical method for fractures mapping and risk zones identification in a coalmine, Northeast, China. *Energy Rep* 7:3785. <https://doi.org/10.1016/j.egy.2021.06.071>
- Khan M, Xueqiu H, Farid A et al (2022) Geophysical characterization of mining-induced complex geological deformations in a deep coalmine. *Lithosphere*. <https://doi.org/10.2113/2022/7564984>
- Khan M, Song D, Shah M, Li Z (2023a) Editorial: evaluation, projection, and prevention of dynamic geological disasters: advances and applications of geophysical methods and numerical modeling. *Front Earth Sci (Lausanne)* 11:1272107
- Khan M, Xueqiu H, Dazhao S et al (2023b) Extracting and predicting rock mechanical behavior based on microseismic spatio-temporal response in an ultra-thick coal seam mine. *Rock Mech Rock Eng* 56:3725. <https://doi.org/10.1007/s00603-023-03247-w>
- Khan M, Xueqiu H, Jia G, Dazhao S (2024) Accurate prediction of indicators for engineering failures in complex mining environments. *Eng Fail Anal* 155:107736. <https://doi.org/10.1016/j.engfailanal.2023.107736>
- Li Z, Tian H, Niu Y et al (2022) Study on the acoustic and thermal response characteristics of coal samples with various prefabricated crack angles during loaded failure under uniaxial compression. *J Appl Geophys* 200:104618. <https://doi.org/10.1016/j.jappgeo.2022.104618>
- Lockner DA, Byerlee JD, Kuksenko V et al (1991) Quasi-static fault growth and shear fracture energy in granite. *Nature* 350:39. <https://doi.org/10.1038/350039a0>
- Lu C, Jiang H, Qu S et al (2022) Hydraulic fracturing design for shale oils based on sweet spot mapping: a case study of the Jimusar formation in China. *J Pet Sci Eng* 214:110568. <https://doi.org/10.1016/j.petrol.2022.110568>
- Meng Q, Zhang M, Han L et al (2016) Effects of acoustic emission and energy evolution of rock specimens under the uniaxial cyclic loading and unloading compression. *Rock Mech Rock Eng* 49:3873. <https://doi.org/10.1007/s00603-016-1077-y>
- Molinda G, Mark C (2010) Ground failures in coal mines with weak roof. *Electron J Geotech Eng* 15(F):547
- Moradian ZA, Ballivy G, Rivard P (2012) Correlating acoustic emission sources with damaged zones during direct shear test of rock joints. *Can Geotech J* 49:710. <https://doi.org/10.1139/T2012-029>
- Pradhan S, Stroisz AM, Fjær E et al (2015) Stress-induced fracturing of reservoir rocks: acoustic monitoring and  $\mu$ CT image analysis. *Rock Mech Rock Eng* 48:2529. <https://doi.org/10.1007/s00603-015-0853-4>
- Shah KR, Labuz JF (1995) Damage mechanisms in stressed rock from acoustic emission. *J Geophys Res* 100:15527. <https://doi.org/10.1029/95jb01236>
- Song D, Wang E, Song X et al (2016) Changes in frequency of electromagnetic radiation from loaded coal rock. *Rock Mech Rock Eng* 49:291. <https://doi.org/10.1007/s00603-015-0738-6>
- Tan Y, Ma Q, Liu X et al (2023) Study on the disaster caused by the linkage failure of the residual coal pillar and rock stratum during multiple coal seam mining: mechanism of progressive and dynamic failure. *Int J Coal Sci Technol* 10:45. <https://doi.org/10.1007/s40789-023-00603-7>
- Tang J, Zhang X, Sun S et al (2022) Evolution characteristics of precursor information of coal and gas outburst in deep rock cross-cut coal uncovering. *Int J Coal Sci Technol* 9:5. <https://doi.org/10.1007/s40789-022-00471-7>
- Vinoth S, Ajay Kumar L (2014) Applying real time seismic monitoring technology for slope stability assessment—An Indian opencast coal mine perspective. *Int J Min Sci Technol* 24:75. <https://doi.org/10.1016/j.ijmst.2013.12.013>
- Wang E, He X, Wei J et al (2011) Electromagnetic emission graded warning model and its applications against coal rock dynamic collapses. *Int J Rock Mech Min Sci* 48:556. <https://doi.org/10.1016/j.ijrmms.2011.02.006>
- Wei H, Hu B, Wang F et al (2020) Temporal-spatial evolution characteristics of acoustic emission in asphalt concrete cracking process under low temperature. *Constr Build Mater* 248:118632. <https://doi.org/10.1016/j.conbuildmat.2020.118632>
- Weiss J (1997) The role of attenuation on acoustic emission amplitude distributions and b-values. *Bull Seismol Soc Am* 87:1362. <https://doi.org/10.1785/bssa0870051362>
- Wong RHC, Chau KT, Tang CA, Lin P (2001) Analysis of crack coalescence in rock-like materials containing three flaws - Part I: Experimental approach. *Int J Rock Mech Min Sci* 38:909. [https://doi.org/10.1016/S1365-1609\(01\)00064-8](https://doi.org/10.1016/S1365-1609(01)00064-8)
- Yan Z, Dai F, Liu Y, Du H (2020) Experimental investigations of the dynamic mechanical properties and fracturing behavior of cracked rocks under dynamic loading. *Bull Eng Geol Environ* 79:5535. <https://doi.org/10.1007/s10064-020-01914-8>
- Zengin E, Erguler ZA (2022) Experimental investigation of pore-fracture relationship on failure behaviour of porous rock materials. *Bull Eng Geol Environ* 81:351. <https://doi.org/10.1007/s10064-022-02857-y>
- Zhang XP, Liu Q, Wu S, Tang X (2015) Crack coalescence between two non-parallel flaws in rock-like material under uniaxial compression. *Eng Geol* 199:74. <https://doi.org/10.1016/j.enggeo.2015.10.007>
- Zhang Z, Wang E, Chen D et al (2016) The observation of AE events under uniaxial compression and the quantitative relationship between the anisotropy index and the main failure plane. *J Appl Geophys* 134:183. <https://doi.org/10.1016/j.jappgeo.2016.09.004>
- Zhang SW, Shou KJ, Xian XF et al (2018a) Fractal characteristics and acoustic emission of anisotropic shale in Brazilian tests. *Tunn Undergr Space Technol* 71:298. <https://doi.org/10.1016/j.tust.2017.08.031>
- Zhang Z, Wang E, Li N et al (2018b) Damage evolution analysis of coal samples under cyclic loading based on single-link cluster

- method. *J Appl Geophys* 152:56–64. <https://doi.org/10.1016/j.jappgeo.2018.03.0145>
- Zhang Z, Liu X, Zhang Y et al (2021) Comparative study on fracture characteristics of coal and rock samples based on acoustic emission technology. *Theor Appl Fract Mech* 111:102851. <https://doi.org/10.1016/j.tafmec.2020.102851>
- Zhao Y, Gao Y, Wu S (2020) Influence of different concealment conditions of parallel double flaws on mechanical properties and failure characteristics of brittle rock under uniaxial compression. *Theor Appl Fract Mech* 109:102751. <https://doi.org/10.1016/j.tafmec.2020.102751>
- Zhao Y, Sun Z, Gao Y et al (2022) Influence of bedding planes on fracture characteristics of coal under mode II loading. *Theor Appl Fract Mech* 117:103131. <https://doi.org/10.1016/j.tafmec.2021.103131>
- Zhao T, Zhang P, Xiao Y et al (2023a) Master crack types and typical acoustic emission characteristics during rock failure. *Int J Coal Sci Technol* 10:2. <https://doi.org/10.1007/s40789-022-00562-5>
- Zhao Y, Liu B, Ling C et al (2023b) Infrared radiation and acoustic emission characteristics of sandstone with different granularities under uniaxial compression. *Bull Eng Geol Environ* 82:24. <https://doi.org/10.1007/s10064-022-03040-z>
- Zhou Z, Zhao C, Cai X, Huang Y (2022) Three-dimensional modeling and analysis of fractal characteristics of rupture source combined acoustic emission and fractal theory. *Chaos Solitons Fractals* 160:112308. <https://doi.org/10.1016/j.chaos.2022.112308>
- Zhou Y, Liu L (2012) Clustering analysis in large graphs with rich attributes. *Intelligent Systems Reference Library* 23:. [https://doi.org/10.1007/978-3-642-23166-7\\_2](https://doi.org/10.1007/978-3-642-23166-7_2)
- Zhurkov SN, Kuksenko VS, Petrov VA (1984) Principles of the kinetic approach of fracture prediction. *Theor Appl Fract Mech* 1:271. [https://doi.org/10.1016/0167-8442\(84\)90007-7](https://doi.org/10.1016/0167-8442(84)90007-7)
- Zöller G, Hainzl S, Kurths J (2001) Observation of growing correlation length as an indicator for critical point behavior prior to large earthquakes. *J Geophys Res Solid Earth* 106:2167. <https://doi.org/10.1029/2000jb900379>

**Publisher's Note** Springer Nature remains neutral with regard to jurisdictional claims in published maps and institutional affiliations.